

Design of Passive and Structural Conductors for Tokamaks Using Thin-Wall Eddy Current Modeling

A.F. Battey¹, C. Hansen¹, D. Garnier², D. Weisberg³, C. Paz-Soldan¹, R. Sweeney⁴, R.A. Tinguely², A.J. Creely⁴

¹ Department of Applied Physics and Math, Columbia University, New York 10027, United States of America

² Massachusetts Institute of Technology, Cambridge, Massachusetts 02139, United States of America

³ General Atomics, San Diego, California 92121, United States of America

⁴ Commonwealth Fusion Systems, Devens, Massachusetts 01434, United States of America

E-mail: a.battey@columbia.edu

January 2023

Abstract. A new three-dimensional electromagnetic modeling tool (*ThinCurr*) has been developed using the existing PSI-Tet finite-element code in support of conducting structure design work for both the SPARC and DIII-D tokamaks. Within this framework a 3D conducting structure model was created for both the SPARC and DIII-D tokamaks in the thin-wall limit. This model includes accurate details of the vacuum vessel and other conducting structural elements with realistic material resistivities. This model was leveraged to support the design of a passive runaway electron mitigation coil (REMC), studying the effect of various design parameters, including coil resistivity, current quench duration, and plasma vertical position, on the effectiveness of the coil. The REMC is a non-axisymmetric coil designed to passively drive large non-axisymmetric fields during the plasma disruption thereby destroying flux surfaces and deconfining RE seed populations. These studies indicate that current designs should apply substantial 3D fields at the plasma surface during future plasma current disruptions as well as highlight the importance of having the REMC conductors away from the machine midplane in order to ensure they are robust to off-normal disruption scenarios.

1. Introduction

Large currents can be induced in tokamak conducting structures in the presence of time-varying magnetic fields, which can be produced by the plasma or external coils. For example, significant induced magnetic fields are generated in the majority of tokamak discharges during the plasma start-up and breakdown phase when currents are ramped quickly in the equilibrium field coils [1]. Changing magnetic fields are also present in tokamak disruptions during the current quench (CQ) as the plasma current

decays rapidly due to a sudden increase in the plasma resistivity after the thermal quench phase[2]. These changing magnetic fields have the ability to generate large electric fields which when coupled with non-axisymmetric features in nearby conducting structures have the potential to drive large non-axisymmetric currents and therefore produce large non-axisymmetric magnetic fields. Non-axisymmetric magnetic fields can have a variety of negative consequences from affecting the null in the equilibrium poloidal field[3], needed for plasma breakdown, to inducing large forces on structures, and potentially driving dangerous magnetohydrodynamic (MHD) instabilities[4]–[6]. However, if properly accounted for, these three-dimensional currents can also be beneficial by slowing the growth rates of MHD instabilities [7]–[12] and deconfining runaway electrons (REs) in the case of runaway electron mitigation coils (REMCs), which are being designed for both the SPARC [13]–[20] and DIII-D [21]–[27] tokamaks. It will be demonstrated in this work that these eddy currents can also significantly affect the response time and efficacy of these REMCs. These potential negative consequences are expected to become more significant in future fusion-relevant machines which will have larger equilibrium magnetic fields and plasma currents, and will therefore be more prone to runaway electrons (REs) and large vessel forces. Therefore, in order to accurately and reliably design and predict the behavior of future devices, it is crucial to be able to simulate the three-dimensional behavior of currents induced in device conducting structures [28]–[32].

The remainder of this paper will be split into five sections. In Section 2, the physics and numerical methods employed by `ThinCurr` are discussed. A study of the proposed REMCs for both the DIII-D and SPARC devices is then presented in Section 3 before a discussion of disruption-induced forces in Section 4. Conclusions and ideas for future work are the discussed in Section 5.

2. ThinCurr: A New 3D Thin-Wall Eddy Current Modeling Tool

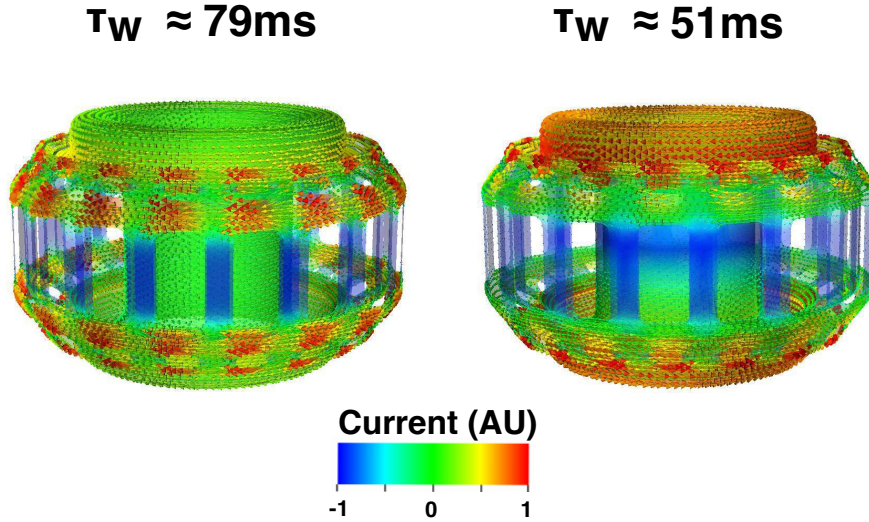


Figure 1. The structure and current decay time-scales of the longest lived (left) and top-down anti-symmetric (right) current patterns for the SPARC vacuum vessel as calculated by the ThinCurr code.

This work utilizes a newly-developed 3D electromagnetic modeling code (ThinCurr), that is based on the PSI-Tet 3D MHD code [33]–[35], and solves a thin-wall eddy current formulation, similar to that used in the VALEN [36] and STARWALL [37] codes, that has proven useful for a variety of electromagnetic applications in fusion [7]–[12], [35], [36], [38]–[42]. However, ThinCurr leverages the modern features of PSI-Tet, such as a CAD interface, the use of unstructured (triangular) grids, parallelization, and interfaces to scalable direct and iterative solvers, to provide additional power and flexibility over prior tools used to study eddy currents in fusion devices. This section provides a brief overview of the code and methods, sufficient to support the presented results. A separate publication will follow with additional information on details of numerical methods and features beyond the scope of this work.

Due to its flexible unstructured finite-element representation, it is straightforward to develop detailed models for 3D conducting structures based on high fidelity CAD models of existing and future machines. The work presented in this article will highlight analysis work completed for both the DIII-D [21] and SPARC tokamaks [17], [20]. An example of the effect of 3D features on calculated current decay time-scales is highlighted in Figure 1 which shows the current distribution (eigenvector) corresponding to the largest eigenvalue ($L\dot{I} = \tau_w RI$) for the SPARC vacuum vessel model computed by ThinCurr. The eigenvector pictured on the left corresponds to the longest lived current pattern, which for a simple torus corresponds to an axisymmetric toroidal current localized on the outboard midplane. Without accounting for three-dimensional features, this current decay time-scale is significantly overestimated by 49.4% when compared to the more

accurate 3D model (118ms (2D) vs 79ms (3D)) shown in figure 1 (left). The shorter time-scale in the 3D case is a consequence of currents being forced to take longer and narrower, and therefore more resistive, current paths as they maneuver around 3D features such as vessel ports.

This difference between the 2D approximation and the full 3D model can be less significant for particular eigenvectors such as the top-bottom anti-symmetric mode shown in Figure 1 (right). This difference (60ms (2D) vs 51ms (3D)) is less than the largest eigenvalue case as the majority of the current flows in the top and bottom of the vessel. These current paths are therefore not forced to change as significantly in the presences of vessel ports, which are primary located at the midplane, and therefore experience comparable resistivities to the 2D approximation. This particular current pattern is important as its decay affects the growth rate of the vertical instability and limits the time-response of external coils in toroidal devices.

For the DIII-D REMC, **ThinCurr** was used to determine the effect of coil radius, and therefore distance from the center-post, on the coil’s performance. The effect of coil resistivity was then explored for the REMCs on both devices. The design robustness of both coils was also verified for the case a varying CQ duration and plasma vertical position during the CQ which could vary during a ‘hot’ vertical displacement event (VDE).

2.1. Model Description

ThinCurr computes the dynamics of currents, subject to inductive coupling and resistive dissipation, on one or more arbitrarily shaped 3D surfaces, corresponding to a thin-wall approximation of conducting regions, and closed filaments. On each surface the current is represented as the rotated gradient of a scalar potential function,

$$\mathbf{J}_s = \mathbf{J} * t_w = \nabla\chi \times \hat{n}, \quad (1)$$

where t_w and \hat{n} are the thickness and unit normal to the surface, respectively. The scalar potential χ is discretized using Lagrange finite elements (FEs) on a triangular mesh. **ThinCurr** supports high order finite element representations, but for this work only linear elements were used. Additional elements are also added to the single-valued Lagrange FE space to enable representation of a multi-valued χ as needed by surfaces with holes and other multiply connected topology.

An L-R circuit model is then defined,

$$L_{ij}\dot{I}_j + R_{ij}I_j = V_i(t), \quad (2)$$

where each “circuit” (i) corresponds to a single basis function in the spatial discretization, whose current forms a divergence free loop by construction. The inductance and resistance matrices can then be computed as

$$L_{ij} = \int \int \frac{(\nabla\chi_i \times \hat{n}) \cdot (\nabla\chi_j \times \hat{n})}{|r' - r|^2} dA' dA \quad (3)$$

and

$$R_{ij} = \int \eta (\nabla \chi_i \times \hat{n}) \cdot (\nabla \chi_j \times \hat{n}) dA \quad (4)$$

respectively, where the resistivity η is defined as a piecewise constant function. Resistivity is allowed to vary between regions in the mesh, which consist of any arbitrary non-overlapping groupings of triangles that are defined via the mesh pre-processor (eg. CUBIT). For the linear elements used in this work, an analytic solution [43] for the potential ($\phi(r) = \int \frac{1}{|r-r'|^2} dA'$) from a triangular element is used to treat the singularity in equation 3.

For currents defined as filaments, the Biot-Savart law is used to replace the inner integration in equation 3. A user-defined radius and resistivity per unit length are used separately to determine self-inductance and resistivity of the filament respectively. Filaments can be defined by a major radius and vertical position pair, for circular coils, or by a collection of 3D points in Cartesian space for arbitrarily-shaped coils. Multiple filaments can be grouped together to represent series wound coils where the current through all windings must be the same. Voltages or currents are then specified in these filaments, which form the source term on the RHS of equation 2.

Several solution types for equation 2 are of interest for conducting structures, primarily the vacuum vessel, in tokamaks and other fusion reactors, including: 1) Time-domain simulations with given initial conditions and $V(t)$ (e.g. disruption simulations), 2) Frequency-domain simulations for the steady state response to oscillatory $V(t) \propto e^{i\omega t}$ (e.g. predicted sensor signals from rotating MHD modes), and 3) Eigenvalue calculations for the characteristic timescales ($\tau_{L/R}$) and modes of the conducting structures (e.g. vertical stability). Both direct and iterative solvers are provided for each type of solution, with parallelized versions available either through libraries (eg. MKL) or internally through PSI-Tet's OpenMP+MPI parallelization. For time-domain calculations a direct solver is often the most efficient approach as the factorization cost is amortized over many time steps, while eigenvalue and frequency-response calculations usually benefit from iterative methods as often only a handful of eigenvalues or a single solve at a given frequency are desired.

For all problem types additional sensors can be defined to measure the magnetic flux through arbitrary closed loops and current flowing across curves in the mesh (cross-sections in the thin-wall limit). Additionally, plot files are saved using HDF5 [44] and Xdmf [45] formats to enable use of VisIt [46] and other tools, to help visualize the 3D structure of currents, magnetic fields, and forces.

ThinCurr can be coupled with professional CAD software to precisely capture important details of potentially complex 3D conductors. For the case of the DIII-D and SPARC tokamaks, their engineering teams maintain highly detailed and accurate CAD models which contain features too small to be captured by a reasonable mesh resolution. Therefore, the first step of developing a **ThinCurr** model is to determine which features will be the most significant for the phenomenon of interest. For the study of disruption and start-up vessel currents this often includes large vessel ports

of 3D structures capable of carry significant currents. The remaining features are then removed with a comparison between the full DIII-D CAD model and the defeatured **ThinCurr** model shown in Figure 2.

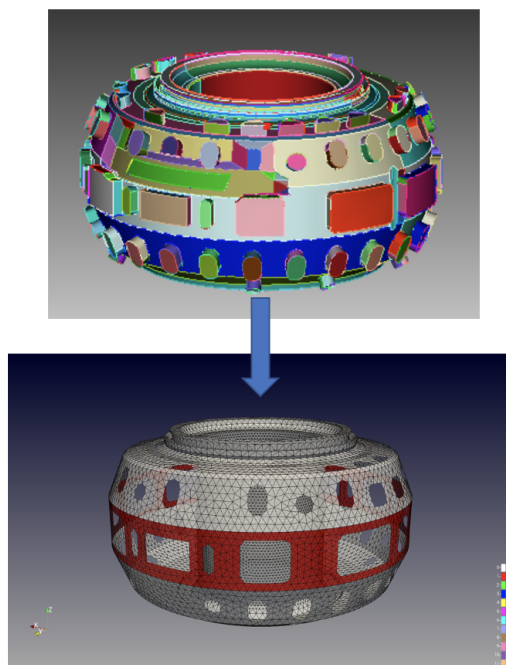


Figure 2. Example of complexity of the original DIII-D CAD model (top) and the **ThinCurr** DIII-D modeling (bottom) following defeaturing to only retain the features which are most important to the phenomenon of interest. The colors in the lower plot represent ‘blocks’ which allow materials with different resistivity or material thickness to be defined.

Regions and individual conductors can then be separately defined to allow different material resistivities to be defined. These differences allow for different materials to be modeled as well as allow the thickness of the conductors to vary across the model. This is the case for both the DIII-D and SPARC vacuum vessel models which are uniform in material but have thicknesses that vary from the high-field to low-field side. An example of these defined regions can be seen in Figure 2 for DIII-D, which has a vessel which is significantly thicker on the low-field side midplane. The thickness of the SPARC vacuum vessel also varies significantly as pictured in Figure 3 as well as the SPARC REMC which is made of a different material.

The model is then triangularly meshed to the desired resolution where it is possible to mesh different regions to higher or lower resolution. This ability was implemented for the DIII-D model whose center-post is modeled with significantly higher resolution due to its proximity to the REMC. Following the meshing all holes in the model must be defined to ensure all flux is accounted for and the final set of equations is well-posed. For example, a simple closed torus would required two holes to be defined: one for the toroidal flux and one for the poloidal flux. These holes correspond to loops around the

minor and major circumference, respectively. Trapped volumes such as those created by a sphere or torus also require a ‘closure mesh’ which corresponds to the removal of an equation from the final equation set [36]. For the case of a closed torus only a single closure is required.

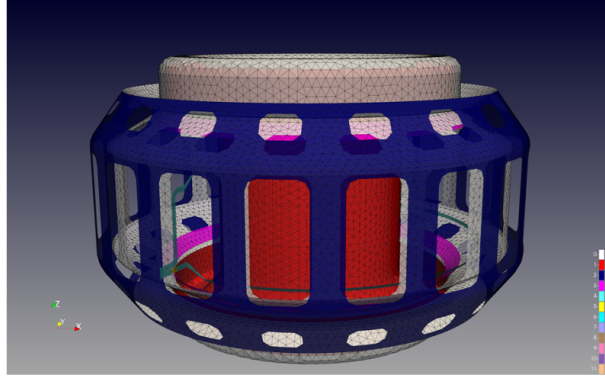


Figure 3. A visualization of the SPARC ThinCurr model where each color represents a different modeled resistivity region. These different resistivities are a result of either different thicknesses or materials.

3. Runaway Electron Mitigation Coil Design

ThinCurr was also leveraged to explore the effectiveness of proposed runaway electron mitigation coils (REMCs) for both the DIII-D and SPARC tokamaks. These coils are passive structures which are designed to prevent and mitigate runaway electrons (REs) which are produced by large loop voltages driven during the CQ phase of tokamak disruptions [31], [47]. These large electric fields are capable of producing REs through two primary mechanisms [30]. Electrons flowing through a hot plasma experience a collisional drag force which is a decreasing function of velocity ($1/v_e^2$) for electrons moving faster than the electron thermal velocity and this force asymptotes for ultra-relativistic electrons at:

$$\frac{4\pi e^4 n \ln \Lambda}{mc^2}, \quad (5)$$

where n is the electron density, m is the electron mass, e is the electron charge, c is the speed of light, and $\ln \Lambda$ is the Coulomb logarithm. Therefore, application of an electron field in excess of the Connor-Hastie field,

$$E_{CH} = \frac{4\pi e^3 n \ln \Lambda}{mc^2}, \quad (6)$$

will eventually produce runaway electrons with unimpeded acceleration of electrons with $v > c\sqrt{E_c/E}$ [48]–[50]. Only a small fraction of the entire electron population falls immediately into the runaway energy range when the electric field is less than the Dreicer field,

$$E_D = \frac{4\pi e^3 n \ln \Lambda}{T}, \quad (7)$$

unless there is a significant hot tail on the electron distribution function.[51]–[54] This hot tail is commonly formed in tokamak disruption plasmas due to an influx of impurities which causes cooling of the hot electrons through collisional drag. Since the higher energy electrons experience fewer collisions they are cooled at a slower rate resulting in surviving “hot-tail” of the initial electron Maxwellian which is strongly susceptible to runaway. The combination of this hot-tail effect and Dreicer production are the primary mechanism for runaway production with these effects dominating in current tokamaks.

The secondary or avalanche mechanism occurs when a thermal electron experiences a hard collision with an existing runaway electron and is bumped into the runaway population while the initial runaway remains in the relativistic population. This effect results in a runaway population which grows exponentially with time as opposed to a linear growth induced by the Dreicer effect [55]. The efficiency of this mechanism scales as an exponential function of the predisturbance plasma current and will therefore dominate along with the hot-tail mechanism for future devices like ITER and SPARC [16], [32], [56]–[60]. In fact this mechanism is expected to be so efficient that it is expected that a considerable fraction of plasma current will be converted directly to RE current unless avoidance methods are implemented.

These RE beams will potentially carry MAs of current, composed of electrons in the MeV range of energies, in future large plasma current devices such as ITER and SPARC. This will pose a serious risk to plasma facing components in future devices. At high plasma currents in ITER RE impacts on the Be limiters could lead to water leaks [61], [62]. SPARC is designed for shorter 10s plasma flattops and does not have active cooling of the tungsten first wall tiles, limiting the worst RE impact failure mode to significant melting [17]. Work remains to assess the space of possible melt damage. Proposed REMCs must be designed to couple to the large disruption-induced loop voltages and apply significant non-axisymmetric fields capable of safely deconfining REs and preventing further RE seed generation. Screening from induced eddy currents, as well as the forces on the overall system, are a crucial factors to consider when evaluating the performance of a potential REMC.

A large effort is therefore underway to determine a method of avoiding REs and, if avoidance is not possible, a method by which the deleterious effects of REs can be safely mitigated [29], [63]–[65]. An exciting candidate for both RE avoidance and mitigation is a passive REMC which takes advantage of the large loop voltage generated by the disruption CQ by placing a non-axisymmetric conductor inside the tokamak vacuum vessel. If this coil is designed properly this loop voltage will drive large currents in the passive conductor which will in turn produce significant non-axisymmetric magnetic fields. Similar 3D fields have been shown both numerically and experimentally to deconfine relativistic electrons by destroying magnetic surfaces [66]–[69], driving large MHD instabilities [19], [70]–[75], and broadening the pitch angle distributions [29], [31],

[47], [64], [66], [76]–[78]. These mechanisms are capable of both preventing the formation of a RE-beam by deconfining seed populations and destroying magnetic surfaces as well as terminating an existing population. Therefore, the effectiveness of the coil is dependent on applying a large 3D field early in the CQ. As a consequence of this, it is crucial to understand potential screening current induced in conductors near the coil which can significantly reduce the magnitude of the applied field at this critical stage.

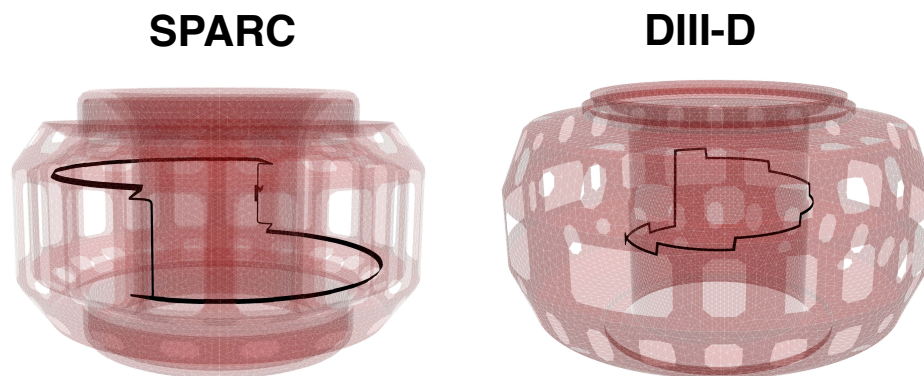


Figure 4. A visualization of the SPARC (left) and DIII-D (right) *ThinCurr* vacuum vessel model in red with the proposed REMC models visualized in black.

As mentioned previously, plasma disruptions are not the only time where large loop voltages are present during a tokamak plasma discharge such as those applied during plasma start-up or from the vertical stability coils (VSCs), which are expected to be located very near the SPARC REMC. There is therefore a risk of the proposed REMC reacting to these various loop voltages and apply unwanted 3D fields. For this reason the REMCs will be able to be placed into an ‘open-circuit’ mode which will prevent current from flowing in the coils. When desired the coils can be returned to their nominal states, where current does not flow until a threshold voltage is reached. This allows passive activation of the coil, while ensuring non-axisymmetric fields are only applied when desired. The REMCs will also be equipped with a variable resistor which will allow both the time-response and maximum voltage to be tailored for a specific research goal.

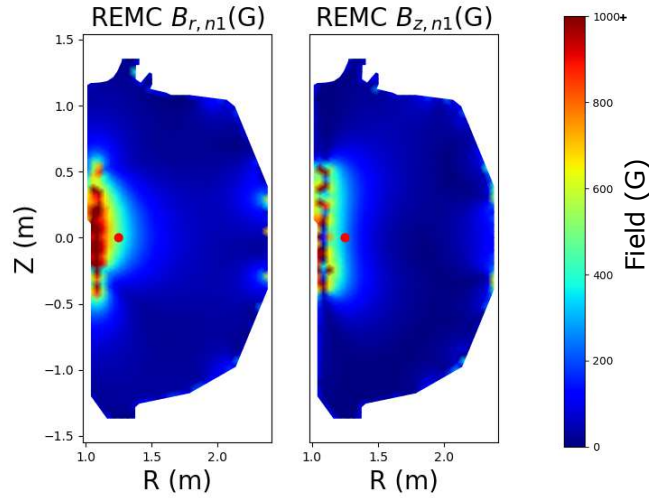


Figure 5. The $n = 1$ field applied by the DIII-D REMC at $t = 18ms$ during a full plasma current disruption with $\tau_{CQ} = 12ms$, where is the CQ begins at $t = 1ms$. The red dot shows the location of the magnetic field measurements shown in later figures.

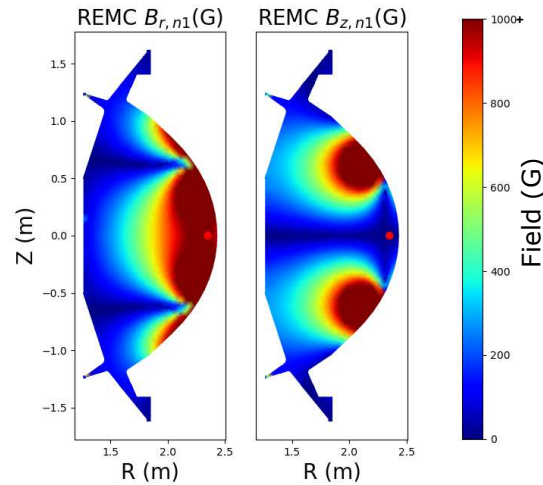


Figure 6. The $n = 1$ field applied by the SPARC REMC at $t = 5ms$ during a full plasma current disruption with $\tau_{CQ} = 3.2ms$, where is the CQ begins at $t = 1ms$. The red dot shows the location of the magnetic field measurements shown in later figures.

The `ThinCurr` code was leveraged to study the effect of screening currents induced in conducting structures near both the DIII-D and SPARC REMCs as well as the ability to inductively couple to the changing plasma current. These screening current effects can vary significantly between devices due to substantial differences in the vacuum vessel resistivities. While both coils are similar in that they are designed to drive a primarily $n=1$ field structure, they differ significantly because the DIII-D coil will be mounted on the high-field (inboard) side near the midplane while the SPARC coil will

be attached to the low-field (outboard) side near the Vertical Stability Coils (VSCs) as shown in Figure 4. These different coil shapes also result in significantly different applied field structures with the radial and vertical fields for the DIII-D and SPARC REMCs shown in Figure 5 and 6, respectively. As a result of these design choices this paper will also serve as a comparison between these two potential mounting locations. Since the performance of the coil depends crucially on its ability to couple to changing currents within the plasma, special attention was paid to how these changing currents were modeled within **ThinCurr**.

A **ThinCurr** model can be driven by prescribing either a voltage or current waveform to a set of predefined filaments. These filaments can be defined by a major radius and vertical position pair or by a collection of points in Cartesian space. The latter provides greater flexibility and the potential to define a coil with 3D features. The most straightforward application involves using a single filament to represent an external magnetic field coil as pictured in Figure 7. As implemented in the SPARC **ThinCurr** model for the central solenoid coils, driven filaments can also be grouped to represent coils with non-negligible height and width. In this case the resolution in both height and width is set by the user with the total coil current shared evenly across the filament set.

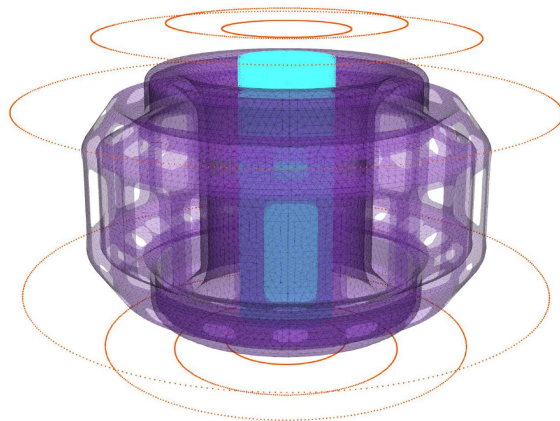


Figure 7. Visualization of the **ThinCurr** model of SPARC including the vacuum vessel (purple), poloidal field coils (orange), and the central solenoid coils (blue).

A more sophisticated driver configuration is used to represent currents flowing in the plasma which was used for all disruption related studies described in this article. In this configuration, circular filaments are laid out in an even rectangular (R-Z) grid with the desired resolution. This grid is then trimmed according to the size and shape of the last closed flux-surface from a reference plasma equilibrium. These filaments are then independently driven to recreate the desired current distribution. These current distributions typically correspond to equilibrium reconstructions from

historical discharges for the DIII-D cases and a target equilibrium for the SPARC cases.

Current in Plasma Filaments (kA)

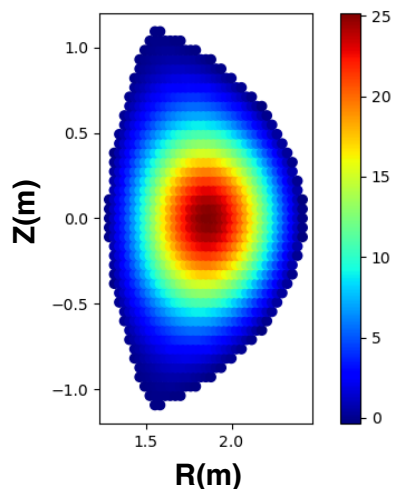


Figure 8. Visualization of current flowing in filaments used to model a SPARC calculated equilibrium current profile in *ThinCurr*. Each colored point corresponds to a different filament in the model with a resolution designed to match that for the equilibrium reconstruction (16.2cm^2).

The currents in the filaments can then be scaled down to simulate a plasma current quench. While the current is scaled the profile can be held rigid or a series of profiles can be provided to allow the structure of the currents to change with time. An example of this technique is shown in Figure 8 for a typical SPARC equilibrium. Note that due to the peakedness of this profile there is significantly less coupling to the wall than a flat profile with identical plasma current and significantly more coupling than using a single filament at the equilibrium current centroid.

Initially the REMC coils were modeled as a single three-dimensional filament; however, in order to capture the effects of the rectangular coil cross-section the coil was instead modeled as a sheet and meshed with a 10cm resolution. This allowed for the cross-sectional height to be accurately captured, and the thickness of the coil is then accounted for by modifying the modeled resistivity. These design choices enabled the coil geometry to accurately match the latest versions of both the SPARC and DIII-D REMCs.

3.1. Effect of Coil Standoff Height - High-Field Side Coil on DIII-D

One consequence of placing the DIII-D coil on the high-field side is that it will be located very near the centerpost vacuum vessel and will therefore experience significant screening from induced eddy currents. As this effect is expected to depend sensitively on the distance between the coil and these conductors, a study was completed on the effect of the height of the coil’s standoff “feet” which will be used to offset the coil from

the vessel. Note that both the coil and desired standoff feet will need to fit underneath the plasma facing tiles, and there is therefore an upper limit on the largest possible standoff of approximately 4cm.

This standoff height was scanned for integer values from one to four centimeters with the results summarized in Figure 9. In the top panel of this figure, the $n=1$ field at the plasma high-field side midplane is shown both with (dashed) and without (solid) screening-current effects. One consequence of a larger standoff height is that the coil is physically closer to the decaying plasma currents and therefore couples to a larger percentage of the pre-disruption current. This can be seen in both the coupling efficiency in Figure 9(bottom) as well as the unscreened field which not only benefits from the increased coil current but also the coil being nearer the measurement location (shown in Figure 5) at the plasma edge. This improved coupling results in a 4.1% increase in the induced current; however, the true parameter of interest is not induced current but the applied magnetic field early in the current quench. This parameter is significantly affected by the inclusion of screening effects which do not significantly affect the maximum field applied by the coil but instead shift this maximum later in time. For simplicity these fields are evaluated at the midpoint of the CQ, which for the simulations presented in Figure 9 corresponds to $t=5\text{ms}$. At this point in the discharge the combination of large screening currents and the coil being physically closer to the plasma results in the 29.6% difference for the radial field and a 31.7% difference of the vertical field between the 1cm and 4cm case. It is therefore recommended that the DIII-D coil be designed with the largest possible standoff allowed by the in-vessel graphite tiles in order to maximize both coupled current and applied non-axisymmetric field.

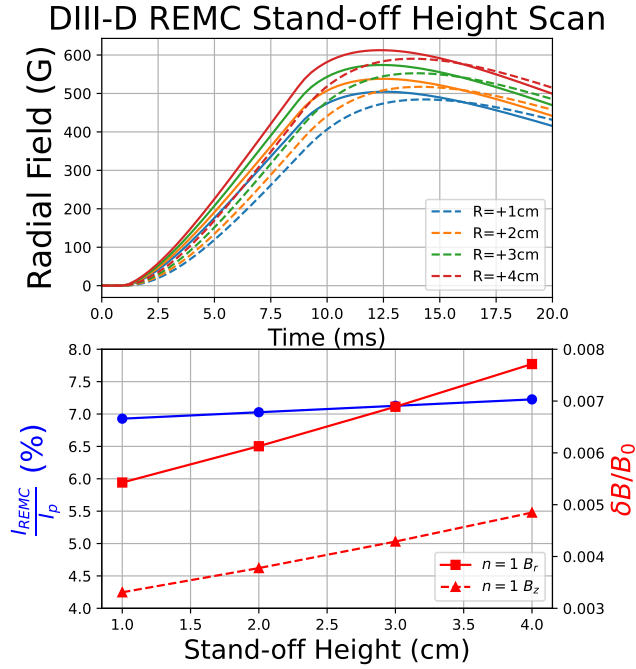


Figure 9. A summary of a study which scanned the distance between the REMC and DIII-D centerpost. The top panel shows the $n = 1$ radial field at the high-field side midplane of the plasma as a function of time with (dashed) and without (solid) eddy current screening. The bottom panel shows the maximum coupling efficiency (blue) and the radial (square) and vertical (triangle) $n = 1$ fields at the midpoint of the CQ ($t=5$ ms). These fields are normalized to the toroidal field at the midplane which is $2.2T$ in this case.

3.2. Effect of Coil Resistance

A study was then completed to determine the effect of the total coil resistance which, as mentioned previously, will be set in experiment using a variable resistor selected by the operator. This was modeled in *ThinCurr* by altering the resistivity of the horizontal connection leg (outside of vacuum vessel) of the coil while the majority of the coil was modeled with a resistance corresponding to height and width of the most up-to-date conductor design. This resistance value was varied from 0.1 mOhm to 100 mOhm for the DIII-D model and 0.1 mOhm to 500 mOhm for the SPARC model. These ranges were picked based on the desire to identify two distinct regimes for coil operation. The first regime will attempt to keep the coil current low for early commissioning and model validation. Once confidence is gained in the design the second regime will attempt to maximize the applied $n = 1$ field while still staying below a maximum allowable current set by structural loading limits.

As expected, the resistance was found to affect both the magnitude and time-dependence of the induced current in the DIII-D REMC. The results of this study including the coupling efficiency and fields applied at the midpoint of the CQ are summarized in Figures 10(b,d). The variable resistor is shown to allow the induced

current to be reduced by several orders of magnitude which will ensure access to both coil operating regimes.

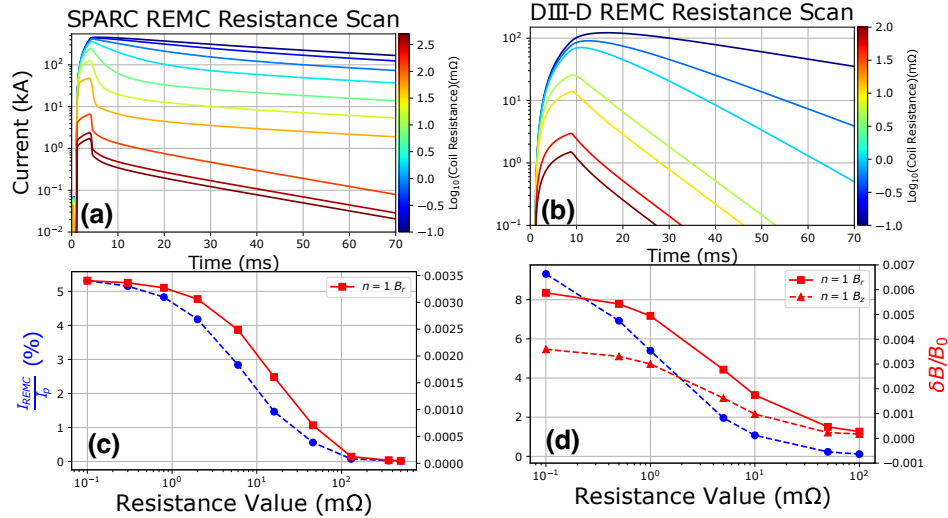


Figure 10. A summary of a study of the effect of coil resistance on the performance of the SPARC and DIII-D REMC. The top plot shows the coil currents as a function of time. The bottom panel shows the coupling efficiency (blue) and the $n = 1$ radial (square) and vertical (triangle) fields at the midpoint of the CQ normalized to the field on axis ($12.2T$ for SPARC and $2.2T$ for DIII-D). Since the vertical field is always near zero for the SPARC coil, with the measurement location shown in Figure 5, it is omitted.

A similar study of the coil resistance was completed for the proposed SPARC REMC and is summarized in Figures 10(a,c). Note that the SPARC REMC applies a much smaller (near zero) vertical field at the vessel midplane and therefore only the radial field varies significantly in this scan. This near zero field is a consequence of cancellation between the fields generated by top and bottom legs of the coil. Due to the significantly higher predischruption plasma current in SPARC, the coil resistance was varied over a slightly larger range in this scan from 0.1 mOhm to 500 mOhm and, similar to the DIII-D case, allows the induced coil current to vary over several orders of magnitude. This large range will allow for distinct commissioning and RE avoidance regimes to be established for this coil and allows hundreds of Gauss to be applied at the plasma early in the CQ when needed [13].

3.3. Effect of Current Quench Duration

Studies were then conducting to evaluate how robust each REMC would be to varying disruption conditions. The first case was motivated by uncertainty of the duration of a typical current quench in SPARC. Since the SPARC tokamak will operate in a unique plasma physics regime where MA runaway beams are expected, an effective and robust REMC is desired to reduce the number of melt events. Therefore, the effect of the CQ

duration on the coil performance parameters was explored using the ThinCurr code. While a well established scaling law allows for confident estimations of the shortest CQ duration, the largest possible values for SPARC are unknown. Therefore, for the study presented here, these values were scanned from the estimated shortest CQ time of $\tau_{CQ} = 3.2\text{ms}$ to a significantly higher upper limit of $\tau_{CQ} = 50\text{ms}$ [16].

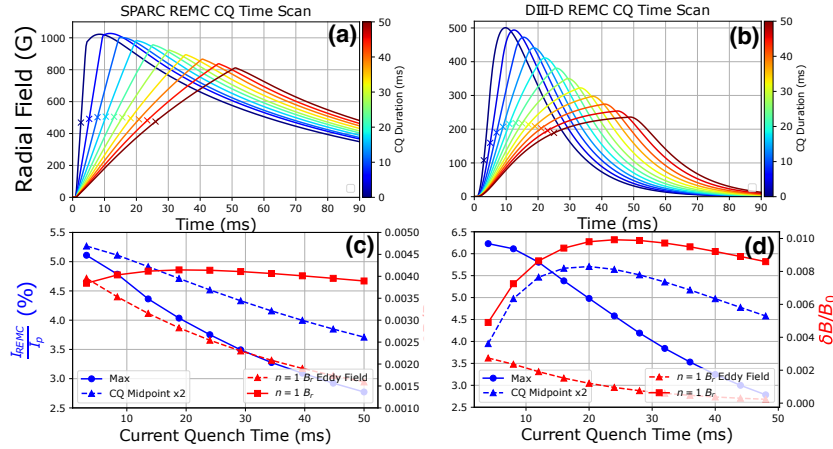


Figure 11. A summary of a study of the effect of current quench duration on the performance of the SPARC (a,c) and DIII-D (b,d) REMC. The top plots show the $n = 1$ radial field at the plasma surface where the colored ‘X’ indicates the halfway point of the current quench. The bottom panel blue points correspond to the coupling efficiency at the maximum value (circles) and at the CQ midpoint (triangles) multiplied by two to allow for a direct comparison. The red points correspond to $n = 1$ radial field at the CQ midpoint from the REMC (squares) and eddy currents (triangles) normalized to the field on axis ($12.2T$ for SPARC and $2.2T$ for DIII-D)

In this study the current profile corresponds to that of a typical 8.7MA SPARC plasma, and this static profile is uniformly decreased linearly with time with a rate corresponding to the τ_{CQ} of interest. A summary of this study is presented in Figures 11(a,c) where the time dependent radial fields, measured at the low-field side midplane, are shown along with the maximum coupled current and applied radial field halfway through the CQ. As expected, the maximum current induced in the coil decreases with CQ duration due to reduced toroidal loop voltage. However, the cases with shorter CQ durations and therefore higher loop voltages also drive significantly larger eddy currents which at the midpoint of the current quench can be quite significant as indicated in Figure 11(c) using the red triangles. Similar to the coil fields, these radial eddy current fields are evaluated as the midpoint of each current quench time. These increased screening currents cancel the field driven by larger currents for faster CQ cases and result in an applied field which is a weak function of CQ time. Therefore, while the total induced current varied by up to 43% in this scan the radial field applied to the plasma varied by less than 5%. This is an unexpected but comforting result that the REMC will be capable of applying large non-axisymmetric fields at the midpoint of

the CQ regardless of the details of the current quench duration for the range of times explored. Also note that while the applied radial fields exceeds 800G for all CQ cases explored only around 500G is applied at this crucial stage.

While the duration of CQs on DIII-D is much better understood, the effect of CQ times on the performance of the DIII-D REMC was also explored using the `ThinCurr` code. This study will allow for further model validation in early experiments implementing the REMC on DIII-D. The results of this study including the time-dependent fields, coupling efficiency, and the coil and eddy current radial fields at $t = \tau_{CQ}/2$ are shown in Figures 11(b,d). One immediate observation is, while CQs were modeled using a linear ramp-down just like the SPARC cases, the time-dependent fields are significantly different shapes due to the proximity of the REMC to the centerpost. Similar to the SPARC cases, the applied radial field has a somewhat unexpected trend. While the coupling efficiency is a quickly decreasing function of τ_{CQ} , the applied radial field has a local maximum near $\tau_{CQ} = 25ms$ with the fastest CQ ($\tau_{CQ} = 4ms$) actually resulting in the lowest radial field for the cases explored.

3.4. Effect of Plasma Vertical Position

Another potential scenario was the possibility of a “hot” vertical displacement event (VDE) which would result in the CQ occurring in a position vertically away from the mid-plane [79]–[87]. Since both the SPARC and DIII-D vacuum vessels are up-down symmetric, the focus of this study was narrowed to consider only upward VDEs, and the plasma cross-section was chosen to be a circle for simplicity. This scenario was modeled assuming that the plasma current does not change significantly during the VDE. Therefore, the CQ can be modeled using a stationary collection of current carrying filaments at the final vertical position with the largest shift corresponding to the highest possible shift without reducing the plasma cross-section. This final position was scanned and the non-axisymmetric fields were measured at the plasma midplane on the side closest to the coil. The measurement locations are indicated using a red ‘X’ in Figures 12 and 13.

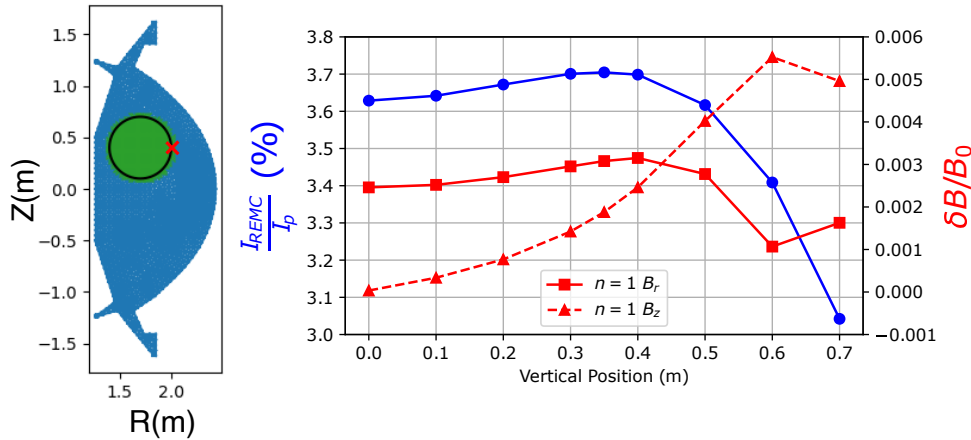


Figure 12. A summary of the effect of plasma vertical position on the performance of the SPARC REMC. The left figure shows an example of a shifted equilibrium ($Z = 0.4\text{m}$) with the measurement location indicated with the red 'X'. The panel on the right shows the coupling efficiency (blue) and sampled $n = 1$ vertical (triangle) and radial (square) fields as a function of vertical position. These fields are normalized to the field on axis (12.2T).

The results of the SPARC coil study are highlighted in Figure 12. As expected, the change in vertical position affects the coils ability to inductively couple to the changing plasma current; however, a bit unexpectedly the maximum coupling does not occur at the center of the vessel and instead occurs near a vertical shift of $\Delta Z = 35\text{cm}$ before falling off. Overall this change in coupling is a minor effect with a maximum difference of 18% in the induced current. This reduction of current for vertical shifts above $\Delta Z = 35\text{cm}$ is more than made up for by the addition of $n=1$ vertical field which grows as the plasma approaches the upper leg of the coil. In fact at the same point as a reduction is seen in the induced current the applied vertical field becomes larger than radial field (exceeds 600G) as the plasma approaches the top of the vessel. Also note that while the vertical motion of the plasma during the VDE will induce a toroidal loop voltage this voltage is not expected to be significant enough to close the switch on the SPARC REMC.

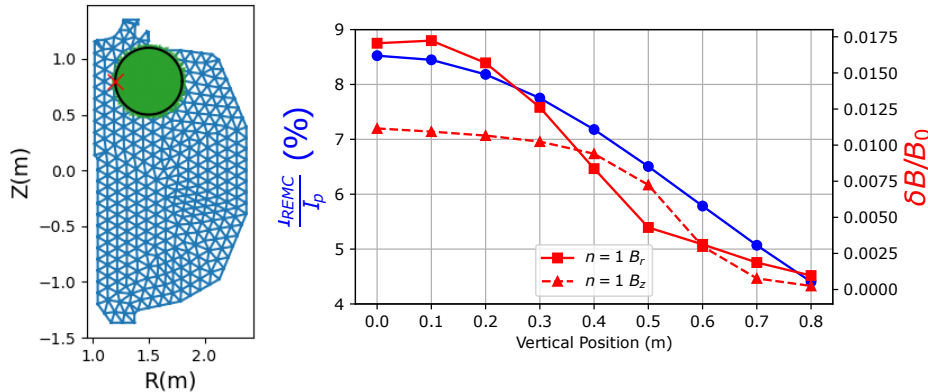


Figure 13. A summary of the effect of plasma vertical position on the performance of the DIII-D REMC. The left figure shows an example of a shifted equilibrium with the measurement location indicated with the red ‘X’. The panel on the right shows the coupling efficiency (blue) and sampled vertical (triangle) and radial (square) fields as a function of vertical position.

The results of a similar study completed for the DIII-D REMC are presented in Figure 13. Similar to the CQ duration study, these results will serve as a useful comparison to potential DIII-D experiments following the installation of the coil which would assess the coil’s performance and robustness as well as serve as a unique opportunity for model validation. Due to the location of the DIII-D coil at the midplane of the DIII-D vacuum vessel centerpost, it experiences a steep drop-off in performance as the CQ occurs at higher vertical positions. This can be seen in the coils, coupling efficiency which drops from 8.52% to 4.40% when the CQ occurs in the top of the vessel. Unlike the SPARC REMC which has the added benefit of a larger $n = 1$ vertical field for higher locations, the DIII-D coil suffers from a two-fold reduction. Not only is there less current induced in the coil, but the plasma is also physically further away which results in both the radial and vertical $n = 1$ fields being reduced to less than 25G for the highest shifted case. At these fields the coil is not expected to be capable of significantly affecting the runaway electron beam. Therefore, these studies indicate that the low-field side coil has a clear advantage in terms of robustness to hot VDEs.

4. REMC and Vacuum Vessel Forces

Due to ThinCurr’s ability to calculate both the eddy current induced in conducting structures and the magnetic fields produced from external coil sets in a fully 3D geometry it is uniquely suited to calculate the $\vec{j} \times \vec{B}$ forces resulting from tokamak disruptions. This is of particular interest for REMCs which will conduct 100s of kAs of current in the presence of large toroidal magnetic fields. The results of these calculations for the DIII-D REMC and vacuum vessel are shown in Figure 14(top), respectively. As expected, the largest forces induced in the horizontal plane are a result of currents flowing in the

longest vertical leg of the coil where the currents are orthogonal to the toroidal magnetic field. This is evident by the angle of the force which points directly at this segment of the coil. Interestingly the largest force on the vacuum vessel during a disruption results from the eddy currents formed in response to the REMC. This force points in the opposite direction to the REMC force but with a significantly lower magnitude. With less than a 1MN of force on both the REMC and vacuum vessel these transient forces should be manageable when properly accounted for.

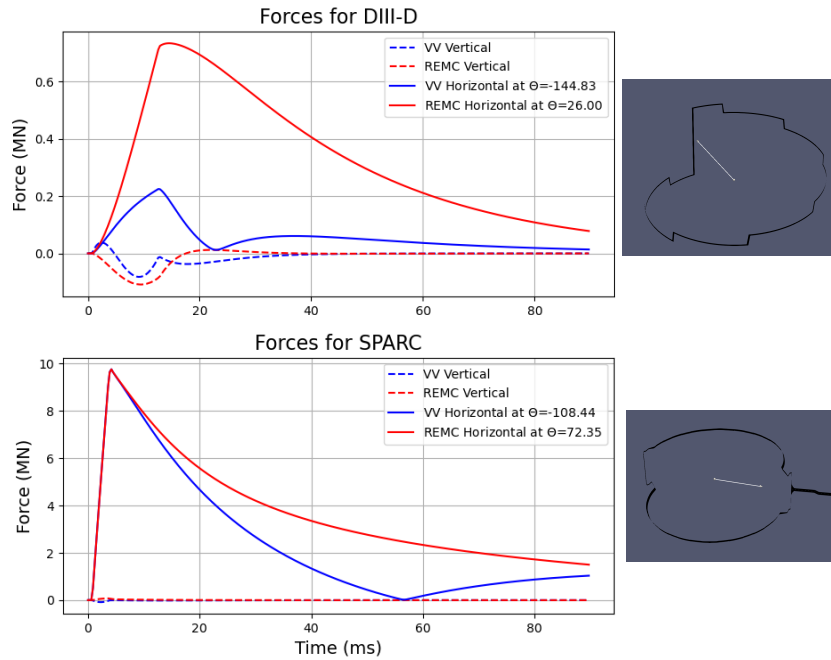


Figure 14. The disruption-induced forces for both the DIII-D and SPARC tokamaks. Shown for both the vacuum vessel due to eddy currents (blue) and REMC (red) with the vertical force shown as a dotted line and horizontal forces shown as a solid line. The horizontal force vector is also shown relative to the REMC in the bottom right.

Due to the significantly larger toroidal field and plasma current in SPARC, it is crucial to accurately predict the forces induced by the REMC and its resulting eddy currents in order to ensure its safe operation. Similar to the DIII-D study the forces calculated by **ThinCurr** are shown in Figure 14(bottom) for both the REMC and vacuum vessel. These forces exceed those predicted for DIII-D by an order of magnitude with forces transiently approaching 10MN. Once again these forces are pointed towards the vertical legs where current flows orthogonal to the magnetic field. The toroidal legs of the coil also interact with the poloidal field (PF) coils, producing a net overturning moment on the vacuum vessel. This will be explored in a future work. An interesting difference from the DIII-D study is that the vessel eddy current and REMC forces are nearly equal and opposite, and since the REMC is supported by the vessel, the net force on the vessel is greatly reduced. This is most likely due to the substantially thicker

and therefore more conducting vacuum vessel where again these forces are a result of eddy currents in response to the REMC fields. The magnitude and direction of these forces as well as any induced torques have to be carefully considered when designing the mounting structures for the coil.

5. Conclusion

The ability to accurately model currents induced in passive conducting structures is a crucial aspect of tokamak design. A newly developed, finite-element, electromagnetic inductive model `ThinCurr` has been leveraged for disruption studies for both the SPARC and DIII-D tokamaks. A highly detailed 3D model was developed for both SPARC and DIII-D within `ThinCurr` including varying material thickness, vessel ports, mounts for the REMC and VSCs (SPARC), and a passive REMC. The fundamental current decay time-scales in the vacuum vessel were found to vary significantly between the fully three-dimensional model and the simplified modeled created by sweeping the 2D cross-section. This further motivated the choice of fully three-dimensional analysis.

Particular attention was then placed on analyzing the effect of various parameters on the performance of the proposed REMC coils for both the SPARC and DIII-D devices. As a consequence of early design choices, this comparison serves as a unique study on the effect of coil location on several key performance parameters with the SPARC coil to be installed on the low-field side and the DIII-D coil on the high-field side. One consequence of the DIII-D REMC's location on the centerpost is that it experiences significant eddy current screening which reduces its ability to apply large fields during the early half of the current quench. This is not expected to limit its effectiveness, but it will be important to offset the coil as much as is allowed by the DIII-D plasma facing tiles.

The performance of the coils was then evaluated as a function of coil resistance which will be set in practice using an external resistor. The range of resistances explored indicate that it will be possible to both reduce the current for the first commissioning phase and maximize the applied fields for RE mitigation and prevention. The robustness of the coils were then evaluated for the case of varying current quench duration and plasma vertical position. Both REMCs were shown to robustly apply significant fields at the midpoint of the CQ regardless of the τ_{CQ} with the somewhat surprising result of slightly larger fields at moderate CQ durations.

The robustness of both coils was also assessed for the case of a hot VDE which would result in the CQ occurring away from the midplane. For the low-field side SPARC coil it was determined that any reduction in coupling efficiency was more than compensated by an increase in $n = 1$ vertical field. The high-field side DIII-D coil showed a much less encouraging result as both the ability to couple to the predisruption plasma current and drive $n = 1$ vertical and radial field quickly diminished as a function of vertical position. This shows a distinct advantage for the low-field side coil in dealing with these types of VDEs.

ThinCurr was then used to calculate the forces induced on both the vacuum vessel and REMC during a plasma current disruption. For both coils this force is a primary consequence of current flowing in the vertical segments of the coil, while the forces on the vessels are a consequence of eddy currents induced in response to the REMC fields. The local forces reacted between the REMC mounts and the vessel were calculated to be less than 1MN for DIII-D and less than 10MN for SPARC. The net body force on the vessel is the sum of the coil force and the vessel eddy current force and these simulations find that it is much reduced relative to the local forces. Engineering efforts are underway to ensure these forces can be tolerated in both devices.

6. Acknowledgments

The work presented in this article was supported through a combination of public and private funds. The results pertaining to the DIII-D tokamak were supported by the U.S. Department of Energy, Office of Science, Office of Fusion Energy Sciences, using the DIII-D National Fusion Facility, a DOE Office of Science user facility, under Award(s) DE-SC0022270, DE-SC0019239, DE-SC0014264, and DE-FC02-04ER54698, while the SPARC studies were supported by Commonwealth Fusion Systems. Some coauthors were supported through a combination of funding sources. A.F. Battey and C. Paz-Soldan were supported by DE-SC0022270 for their work relating to the DIII-D device and Commonwealth Fusion Systems for the work on the SPARC machine. Similarly, R. Sweeney was supported by DE-SC0014264 for collaboration on the DIII-D studies and by Commonwealth Fusion Systems for the SPARC REMC studies and C. Hansen was supported by DE-SC0019239 for work related to ThinCurr model development and DIII-D studies and by Commonwealth Fusion Systems for all SPARC research. D. Garnier, R.A. Tinguely, and A.J. Creely were supported entirely by Commonwealth Fusion systems while D. Weisberg was supported entirely through DE-FC02-04ER54698.

Disclaimer: This report was prepared as an account of work sponsored by an agency of the United States Government. Neither the United States Government nor any agency thereof, nor any of their employees, makes any warranty, express or implied, or assumes any legal liability or responsibility for the accuracy, completeness, or usefulness of any information, apparatus, product, or process disclosed, or represents that its use would not infringe privately owned rights. Reference herein to any specific commercial product, process, or service by trade name, trademark, manufacturer, or otherwise does not necessarily constitute or imply its endorsement, recommendation, or favoring by the United States Government or any agency thereof. The views and opinions of authors expressed herein do not necessarily state or reflect those of the United States Government or any agency thereof.

References

- [1] Maxwell, James C., “On faraday’s lines of force,” *Cambridge Philosophical Society Transactions*, pp. 27–83, 1855.
- [2] J. A. Wesson, R. D. Gill, M. Hugon, *et al.*, “Disruptions in JET,” *Nuclear Fusion*, vol. 29, no. 4, p. 641, Apr. 1989, ISSN: 0029-5515. DOI: 10.1088/0029-5515/29/4/009. [Online]. Available: <https://dx.doi.org/10.1088/0029-5515/29/4/009> (visited on 05/09/2023).
- [3] V. D. Pustovitov, “Models and scalings for the disruption forces in tokamaks,” *Nuclear Fusion*, vol. 62, no. 2, p. 026 036, Jan. 2022, Publisher: IOP Publishing, ISSN: 0029-5515. DOI: 10.1088/1741-4326/ac3fe9. [Online]. Available: <https://dx.doi.org/10.1088/1741-4326/ac3fe9> (visited on 05/09/2023).
- [4] G. L. Jackson, T. A. Casper, T. C. Luce, *et al.*, “ITER startup studies in the DIII-d tokamak,” *Nuclear Fusion*, vol. 48, no. 12, p. 125 002, Nov. 2008, ISSN: 0029-5515. DOI: 10.1088/0029-5515/48/12/125002. [Online]. Available: <https://dx.doi.org/10.1088/0029-5515/48/12/125002> (visited on 05/10/2023).
- [5] G. L. Jackson, T. A. Casper, T. C. Luce, *et al.*, “Simulating ITER plasma startup and rampdown scenarios in the DIII-d tokamak,” *Nuclear Fusion*, vol. 49, no. 11, p. 115 027, Oct. 2009, ISSN: 0029-5515. DOI: 10.1088/0029-5515/49/11/115027. [Online]. Available: <https://dx.doi.org/10.1088/0029-5515/49/11/115027> (visited on 05/10/2023).
- [6] J. A. Leuer, N. W. Eidietis, J. R. Ferron, *et al.*, “Plasma startup design of fully superconducting tokamaks EAST and KSTAR with implications for ITER,” *IEEE Transactions on Plasma Science*, vol. 38, no. 3, pp. 333–340, Mar. 2010, Conference Name: IEEE Transactions on Plasma Science, ISSN: 1939-9375. DOI: 10.1109/TPS.2009.2037890.
- [7] A. H. Boozer, “Simplified multimode calculations of resistive wall modes,” *Physics of Plasmas*, vol. 17, no. 7, p. 072 503, Jul. 2010, Publisher: American Institute of Physics, ISSN: 1070-664X. DOI: 10.1063/1.3453706. [Online]. Available: <https://aip-scitation-org.ezproxy.cul.columbia.edu/doi/10.1063/1.3453706> (visited on 01/18/2023).
- [8] M. Clement, J. Hanson, J. Bialek, and G. Navratil, “GPU-based optimal control for RWM feedback in tokamaks,” *Control Engineering Practice*, vol. 68, pp. 15–22, Nov. 1, 2017, ISSN: 0967-0661. DOI: 10.1016/j.conengprac.2017.08.002. [Online]. Available: <https://www.sciencedirect.com/science/article/pii/S0967066117301685> (visited on 01/18/2023).
- [9] M. Clement, J. Hanson, J. Bialek, and G. Navratil, “Optimal control techniques for resistive wall mode feedback in tokamaks,” *Nuclear Fusion*, vol. 58, no. 4, p. 046 017, Feb. 2018, Publisher: IOP Publishing, ISSN: 0029-5515. DOI: 10.1088/1741-4326/aaaecd. [Online]. Available: <https://dx.doi.org/10.1088/1741-4326/aaaecd> (visited on 01/18/2023).

- [10] M. E. Mauel, J. Bialek, A. H. Boozer, *et al.*, “Dynamics and control of resistive wall modes with magnetic feedback control coils: Experiment and theory,” *Nuclear Fusion*, vol. 45, no. 4, p. 285, Apr. 2005, ISSN: 0029-5515. DOI: 10.1088/0029-5515/45/4/010. [Online]. Available: <https://dx.doi.org/10.1088/0029-5515/45/4/010> (visited on 01/18/2023).
- [11] M. Okabayashi, J. Bialek, A. Bondeson, *et al.*, “Control of the resistive wall mode with internal coils in the DIII-d tokamak,” *Nuclear Fusion*, vol. 45, no. 12, p. 1715, Nov. 2005, ISSN: 0029-5515. DOI: 10.1088/0029-5515/45/12/028. [Online]. Available: <https://dx.doi.org/10.1088/0029-5515/45/12/028> (visited on 01/18/2023).
- [12] A. F. Battey, J. M. Hanson, J. Bialek, F. Turco, G. A. Navratil, and N. C. Logan, “Simultaneous stabilization and control of the $n = 1$ and $n = 2$ resistive wall mode,” *Nuclear Fusion*, vol. 63, no. 6, p. 066025, Apr. 2023, Publisher: IOP Publishing, ISSN: 0029-5515. DOI: 10.1088/1741-4326/accd81. [Online]. Available: <https://dx.doi.org/10.1088/1741-4326/accd81> (visited on 05/08/2023).
- [13] V. A. Izzo, I. Pusztai, K. Särkimäki, *et al.*, “Runaway electron deconfinement in SPARC and DIII-d by a passive 3d coil,” *Nuclear Fusion*, vol. 62, no. 9, p. 096029, Aug. 2022, Publisher: IOP Publishing, ISSN: 0029-5515. DOI: 10.1088/1741-4326/ac83d8. [Online]. Available: <https://dx.doi.org/10.1088/1741-4326/ac83d8> (visited on 05/08/2023).
- [14] R. A. Tinguely, I. Pusztai, V. A. Izzo, *et al.*, “On the minimum transport required to passively suppress runaway electrons in SPARC disruptions,” *Plasma Physics and Controlled Fusion*, vol. 65, no. 3, p. 034002, Jan. 2023, Publisher: IOP Publishing, ISSN: 0741-3335. DOI: 10.1088/1361-6587/acb083. [Online]. Available: <https://dx.doi.org/10.1088/1361-6587/acb083> (visited on 05/08/2023).
- [15] R. A. Tinguely, V. A. Izzo, D. T. Garnier, *et al.*, “Modeling the complete prevention of disruption-generated runaway electron beam formation with a passive 3d coil in SPARC,” *Nuclear Fusion*, vol. 61, no. 12, p. 124003, Nov. 2021, Publisher: IOP Publishing, ISSN: 0029-5515. DOI: 10.1088/1741-4326/ac31d7. [Online]. Available: <https://dx.doi.org/10.1088/1741-4326/ac31d7> (visited on 05/08/2023).
- [16] R. Sweeney, A. J. Creely, J. Doody, *et al.*, “MHD stability and disruptions in the SPARC tokamak,” *Journal of Plasma Physics*, vol. 86, no. 5, p. 865860507, Oct. 2020, Publisher: Cambridge University Press, ISSN: 0022-3778, 1469-7807. DOI: 10.1017/S0022377820001129. [Online]. Available: <https://www.cambridge.org/core/journals/journal-of-plasma-physics/article/mhd-stability-and-disruptions-in-the-sparc-tokamak/908C6788COD625C5DDF335DBD9A17476> (visited on 05/08/2023).

- [17] A. J. Creely, M. J. Greenwald, S. B. Ballinger, *et al.*, “Overview of the SPARC tokamak,” *Journal of Plasma Physics*, vol. 86, no. 5, p. 865 860 502, Oct. 2020, Publisher: Cambridge University Press, ISSN: 0022-3778, 1469-7807. DOI: 10 . 1017/S0022377820001257. [Online]. Available: <https://www.cambridge.org/core/journals/journal-of-plasma-physics/article/overview-of-the-sparc-tokamak/DD3C44ECD26F5EACC554811764EF9FF0> (visited on 05/04/2023).
- [18] P. Rodriguez-Fernandez, A. J. Creely, M. J. Greenwald, *et al.*, “Overview of the SPARC physics basis towards the exploration of burning-plasma regimes in high-field, compact tokamaks,” *Nuclear Fusion*, vol. 62, no. 4, p. 042 003, Mar. 2022, Publisher: IOP Publishing, ISSN: 0029-5515. DOI: 10.1088/1741-4326/ac1654. [Online]. Available: <https://dx.doi.org/10.1088/1741-4326/ac1654> (visited on 05/08/2023).
- [19] V. A. Izzo, D. A. Humphreys, and M. Kornbluth, “Analysis of shot-to-shot variability in post-disruption runaway electron currents for diverted DIII-d discharges,” *Plasma Physics and Controlled Fusion*, vol. 54, no. 9, p. 095 002, Jul. 2012, Publisher: IOP Publishing, ISSN: 0741-3335. DOI: 10 . 1088 / 0741 - 3335/54/9/095002. [Online]. Available: <https://dx.doi.org/10.1088/0741-3335/54/9/095002> (visited on 05/08/2023).
- [20] M. Greenwald, “Status of the SPARC physics basis,” *Journal of Plasma Physics*, vol. 86, no. 5, p. 861 860 501, Oct. 2020, Publisher: Cambridge University Press, ISSN: 0022-3778, 1469-7807. DOI: 10.1017/S0022377820001063. [Online]. Available: <https://www.cambridge.org/core/journals/journal-of-plasma-physics/article/status-of-the-sparc-physics-basis/B21625B93C0654B955B776566C96DF6B> (visited on 05/08/2023).
- [21] J. L. Luxon, “A design retrospective of the DIII-d tokamak,” *Nuclear Fusion*, vol. 42, no. 5, p. 614, May 2002, ISSN: 0029-5515. DOI: 10.1088/0029-5515/42/5/313. [Online]. Available: <https://dx.doi.org/10.1088/0029-5515/42/5/313> (visited on 05/08/2023).
- [22] N. Commaux, L. R. Baylor, S. K. Combs, *et al.*, “Novel rapid shutdown strategies for runaway electron suppression in DIII-d,” *Nuclear Fusion*, vol. 51, no. 10, p. 103 001, Aug. 2011, ISSN: 0029-5515. DOI: 10.1088/0029-5515/51/10/103001. [Online]. Available: <https://dx.doi.org/10.1088/0029-5515/51/10/103001> (visited on 05/08/2023).
- [23] E. M. Hollmann, N. Commaux, N. W. Eidietis, *et al.*, “Experiments in DIII-d toward achieving rapid shutdown with runaway electron suppression),” *Physics of Plasmas*, vol. 17, no. 5, p. 056 117, May 6, 2010, ISSN: 1070-664X. DOI: 10 . 1063/1.3309426. [Online]. Available: <https://doi.org/10.1063/1.3309426> (visited on 05/08/2023).
- [24] N. W. Eidietis, N. Commaux, E. M. Hollmann, *et al.*, “Control of post-disruption runaway electron beams in DIII-da),” *Physics of Plasmas*, vol. 19, no. 5, p. 056 109,

- Mar. 28, 2012, ISSN: 1070-664X. DOI: 10.1063/1.3695000. [Online]. Available: <https://doi.org/10.1063/1.3695000> (visited on 05/08/2023).
- [25] P. L. Taylor, A. G. Kellman, T. E. Evans, *et al.*, “Disruption mitigation studies in DIII-d,” *Physics of Plasmas*, vol. 6, no. 5, pp. 1872–1879, May 1, 1999, ISSN: 1070-664X. DOI: 10.1063/1.873445. [Online]. Available: <https://doi.org/10.1063/1.873445> (visited on 05/08/2023).
- [26] D. Shiraki, N. Commaux, L. R. Baylor, *et al.*, “Dissipation of post-disruption runaway electron plateaus by shattered pellet injection in DIII-d,” *Nuclear Fusion*, vol. 58, no. 5, p. 056006, Mar. 2018, Publisher: IOP Publishing, ISSN: 0029-5515. DOI: 10.1088/1741-4326/aab0d6. [Online]. Available: <https://dx.doi.org/10.1088/1741-4326/aab0d6> (visited on 05/08/2023).
- [27] D. B. Weisberg, C. Paz-Soldan, Y. Q. Liu, A. Welander, and C. Dunn, “Passive deconfinement of runaway electrons using an in-vessel helical coil,” *Nuclear Fusion*, vol. 61, no. 10, p. 106033, Sep. 2021, Publisher: IOP Publishing, ISSN: 0029-5515. DOI: 10.1088/1741-4326/ac2279. [Online]. Available: <https://dx.doi.org/10.1088/1741-4326/ac2279> (visited on 05/08/2023).
- [28] P. C. ITER Physics Expert Group on Disruptions, MHD, and I. P. B. Editors, “Chapter 3: MHD stability, operational limits and disruptions,” *Nuclear Fusion*, vol. 39, no. 12, p. 2251, Dec. 1999, ISSN: 0029-5515. DOI: 10.1088/0029-5515/39/12/303. [Online]. Available: <https://dx.doi.org/10.1088/0029-5515/39/12/303> (visited on 05/09/2023).
- [29] M. Lehnen, K. Aleynikova, P. B. Aleynikov, *et al.*, “Disruptions in ITER and strategies for their control and mitigation,” *Journal of Nuclear Materials, PLASMA-SURFACE INTERACTIONS* 21, vol. 463, pp. 39–48, Aug. 1, 2015, ISSN: 0022-3115. DOI: 10.1016/j.jnucmat.2014.10.075. [Online]. Available: <https://www.sciencedirect.com/science/article/pii/S0022311514007594> (visited on 05/08/2023).
- [30] B. N. Breizman, P. Aleynikov, E. M. Hollmann, and M. Lehnen, “Physics of runaway electrons in tokamaks,” *Nuclear Fusion*, vol. 59, no. 8, p. 083001, Jun. 2019, Publisher: IOP Publishing, ISSN: 0029-5515. DOI: 10.1088/1741-4326/ab1822. [Online]. Available: <https://dx.doi.org/10.1088/1741-4326/ab1822> (visited on 01/25/2023).
- [31] A. H. Boozer, “Two beneficial non-axisymmetric perturbations to tokamaks,” *Plasma Physics and Controlled Fusion*, vol. 53, no. 8, p. 084002, May 2011, ISSN: 0741-3335. DOI: 10.1088/0741-3335/53/8/084002. [Online]. Available: <https://dx.doi.org/10.1088/0741-3335/53/8/084002> (visited on 05/08/2023).
- [32] A. H. Boozer, “Runaway electrons and ITER,” *Nuclear Fusion*, vol. 57, no. 5, p. 056018, Mar. 2017, Publisher: IOP Publishing, ISSN: 0029-5515. DOI: 10.1088/1741-4326/aa6355. [Online]. Available: <https://dx.doi.org/10.1088/1741-4326/aa6355> (visited on 05/09/2023).

- [33] C. J. Hansen, “MHD modeling in complex 3d geometries: Towards predictive simulation of SIHI current drive,” Accepted: 2014-04-30T16:21:50Z, Thesis, Apr. 30, 2014. [Online]. Available: <https://digital.lib.washington.edu:443/researchworks/handle/1773/25420> (visited on 05/09/2023).
- [34] C. Hansen, B. Victor, K. Morgan, *et al.*, “Numerical studies and metric development for validation of magnetohydrodynamic models on the HIT-SI experimenta),” *Physics of Plasmas*, vol. 22, no. 5, p. 056 105, Apr. 27, 2015, ISSN: 1070-664X. DOI: 10.1063/1.4919277. [Online]. Available: <https://doi.org/10.1063/1.4919277> (visited on 05/09/2023).
- [35] A. H. Boozer, “Equations for studies of feedback stabilization,” *Physics of Plasmas*, vol. 5, no. 9, pp. 3350–3357, Sep. 1, 1998, ISSN: 1070-664X. DOI: 10.1063/1.873048. [Online]. Available: <https://doi.org/10.1063/1.873048> (visited on 05/09/2023).
- [36] J. Bialek, A. H. Boozer, M. E. Mauel, and G. A. Navratil, “Modeling of active control of external magnetohydrodynamic instabilities,” *Physics of Plasmas*, vol. 8, no. 5, pp. 2170–2180, May 2001, Publisher: American Institute of Physics, ISSN: 1070-664X. DOI: 10.1063/1.1362532. [Online]. Available: <https://aip-scitation-org.ezproxy.cul.columbia.edu/doi/10.1063/1.1362532> (visited on 01/18/2023).
- [37] P. Merkel and E. Strumberger, *Linear MHD stability studies with the STARWALL code*, Aug. 20, 2015. DOI: 10.48550/arXiv.1508.04911. arXiv: 1508.04911[physics]. [Online]. Available: <http://arxiv.org/abs/1508.04911> (visited on 05/30/2023).
- [38] A. H. Boozer, “Resistive wall modes and error field amplification,” *Physics of Plasmas*, vol. 10, no. 5, pp. 1458–1467, May 2003, Publisher: American Institute of Physics, ISSN: 1070-664X. DOI: 10.1063/1.1568751. [Online]. Available: <https://aip-scitation-org.ezproxy.cul.columbia.edu/doi/10.1063/1.1568751> (visited on 01/18/2023).
- [39] A. H. Boozer, “Stabilization of resistive wall modes by slow plasma rotation,” *Physics of Plasmas*, vol. 2, no. 12, pp. 4521–4532, Dec. 1995, Publisher: American Institute of Physics, ISSN: 1070-664X. DOI: 10.1063/1.871009. [Online]. Available: <https://aip-scitation-org.ezproxy.cul.columbia.edu/doi/10.1063/1.871009> (visited on 01/18/2023).
- [40] O. Katsuro-Hopkins, J. Bialek, D. A. Maurer, and G. A. Navratil, “Enhanced ITER resistive wall mode feedback performance using optimal control techniques,” *Nuclear Fusion*, vol. 47, no. 9, p. 1157, Aug. 2007, ISSN: 0029-5515. DOI: 10.1088/0029-5515/47/9/012. [Online]. Available: <https://dx.doi.org/10.1088/0029-5515/47/9/012> (visited on 01/18/2023).

- [41] J. M. Hanson, J. Bialek, F. Turco, *et al.*, “Validation of conducting wall models using magnetic measurements,” *Nuclear Fusion*, vol. 56, no. 10, p. 106 022, Aug. 2016, Publisher: IOP Publishing, ISSN: 0029-5515. DOI: 10.1088/0029-5515/56/10/106022. [Online]. Available: <https://dx.doi.org/10.1088/0029-5515/56/10/106022> (visited on 01/18/2023).
- [42] A. H. Boozer, “Robust feedback systems for resistive wall modes,” *Physics of Plasmas*, vol. 11, no. 1, pp. 110–114, Jan. 2004, Publisher: American Institute of Physics, ISSN: 1070-664X. DOI: 10.1063/1.1628687. [Online]. Available: <https://aip-scitation-org.ezproxy.cul.columbia.edu/doi/10.1063/1.1628687> (visited on 01/18/2023).
- [43] A. Ferguson, X. Zhang, and G. Stroink, “A complete linear discretization for calculating the magnetic field using the boundary element method,” *IEEE Transactions on Biomedical Engineering*, vol. 41, no. 5, pp. 455–460, 1994. DOI: 10.1109/10.293220.
- [44] “HDF5: HDF5 reference manual.” (), [Online]. Available: https://docs.hdfgroup.org/hdf5/develop/_r_m.html (visited on 05/09/2023).
- [45] “XDMF model and format - XdmfWeb.” (), [Online]. Available: https://www.xdmf.org/index.php/XDMF_Model_and_Format (visited on 05/09/2023).
- [46] “Citing VisIt,” VisIt Home. (), [Online]. Available: <https://visit-dav.github.io/visit-website/citing-visit/> (visited on 05/09/2023).
- [47] H. M. Smith, A. H. Boozer, and P. Helander, “Passive runaway electron suppression in tokamak disruptions,” *Physics of Plasmas*, vol. 20, no. 7, p. 072 505, Jul. 24, 2013, ISSN: 1070-664X. DOI: 10.1063/1.4813255. [Online]. Available: <https://doi.org/10.1063/1.4813255> (visited on 05/08/2023).
- [48] J. W. Connor and R. J. Hastie, “Relativistic limitations on runaway electrons,” *Nuclear Fusion*, vol. 15, no. 3, p. 415, Jun. 1975, ISSN: 0029-5515. DOI: 10.1088/0029-5515/15/3/007. [Online]. Available: <https://dx.doi.org/10.1088/0029-5515/15/3/007> (visited on 02/07/2023).
- [49] H. Dreicer, “Electron and ion runaway in a fully ionized gas. I,” *Physical Review*, vol. 115, no. 2, pp. 238–249, Jul. 15, 1959, Publisher: American Physical Society. DOI: 10.1103/PhysRev.115.238. [Online]. Available: <https://link.aps.org/doi/10.1103/PhysRev.115.238> (visited on 01/18/2023).
- [50] H. Dreicer, “Electron and ion runaway in a fully ionized gas. II,” *Physical Review*, vol. 117, no. 2, pp. 329–342, Jan. 15, 1960, Publisher: American Physical Society. DOI: 10.1103/PhysRev.117.329. [Online]. Available: <https://link.aps.org/doi/10.1103/PhysRev.117.329> (visited on 01/18/2023).
- [51] I. Svenningsson, O. Embreus, M. Hoppe, S. L. Newton, and T. Fülöp, “Hot-tail runaway seed landscape during the thermal quench in tokamaks,” *Physical Review Letters*, vol. 127, no. 3, p. 035 001, Jul. 14, 2021, Publisher: American Physical Society. DOI: 10.1103/PhysRevLett.127.035001. [Online]. Available:

- <https://link.aps.org/doi/10.1103/PhysRevLett.127.035001> (visited on 05/08/2023).
- [52] H. M. Smith and E. Verwichte, “Hot tail runaway electron generation in tokamak disruptions,” *Physics of Plasmas*, vol. 15, no. 7, p. 072502, Jul. 2008, Publisher: American Institute of Physics, ISSN: 1070-664X. DOI: 10.1063/1.2949692. [Online]. Available: <https://aip-scitation-org.ezproxy.cul.columbia.edu/doi/10.1063/1.2949692> (visited on 01/18/2023).
- [53] P. Aleynikov and B. N. Breizman, “Generation of runaway electrons during the thermal quench in tokamaks,” *Nuclear Fusion*, vol. 57, no. 4, p. 046009, Feb. 2017, Publisher: IOP Publishing, ISSN: 0029-5515. DOI: 10.1088/1741-4326/aa5895. [Online]. Available: <https://dx.doi.org/10.1088/1741-4326/aa5895> (visited on 05/08/2023).
- [54] E. M. Hollmann, N. Commaux, N. W. Eidietis, *et al.*, “Study of z scaling of runaway electron plateau final loss energy deposition into wall of DIII-d,” *Physics of Plasmas*, vol. 24, no. 6, p. 062505, Jun. 12, 2017, ISSN: 1070-664X. DOI: 10.1063/1.4985086. [Online]. Available: <https://doi.org/10.1063/1.4985086> (visited on 05/08/2023).
- [55] M. N. Rosenbluth and S. V. Putvinski, “Theory for avalanche of runaway electrons in tokamaks,” *Nuclear Fusion*, vol. 37, no. 10, p. 1355, Oct. 1997, ISSN: 0029-5515. DOI: 10.1088/0029-5515/37/10/I03. [Online]. Available: <https://dx.doi.org/10.1088/0029-5515/37/10/I03> (visited on 01/18/2023).
- [56] F. Saint-Laurent, G. Martin, T. Alarcon, *et al.*, “Overview of runaway electron control and mitigation experiments on tore supra and lessons learned in view of ITER,” *Fusion Science and Technology*, vol. 64, no. 4, pp. 711–718, Nov. 1, 2013, Publisher: Taylor & Francis eprint: <https://doi.org/10.13182/FST13-A24090>, ISSN: 1536-1055. DOI: 10.13182/FST13-A24090. [Online]. Available: <https://doi.org/10.13182/FST13-A24090> (visited on 05/09/2023).
- [57] E. Nilsson, J. Decker, Y. Peysson, R. S. Granetz, F. Saint-Laurent, and M. Vlaine, “Kinetic modelling of runaway electron avalanches in tokamak plasmas,” *Plasma Physics and Controlled Fusion*, vol. 57, no. 9, p. 095006, Jul. 2015, Publisher: IOP Publishing, ISSN: 0741-3335. DOI: 10.1088/0741-3335/57/9/095006. [Online]. Available: <https://dx.doi.org/10.1088/0741-3335/57/9/095006> (visited on 05/09/2023).
- [58] C. J. McDevitt, Z. Guo, and X.-Z. Tang, “Avalanche mechanism for runaway electron amplification in a tokamak plasma,” *Plasma Physics and Controlled Fusion*, vol. 61, no. 5, p. 054008, Apr. 2019, Publisher: IOP Publishing, ISSN: 0741-3335. DOI: 10.1088/1361-6587/ab0d6d. [Online]. Available: <https://dx.doi.org/10.1088/1361-6587/ab0d6d> (visited on 05/09/2023).

- [59] J. R. Martín-Solís, A. Loarte, and M. Lehnen, “Formation and termination of runaway beams in ITER disruptions,” *Nuclear Fusion*, vol. 57, no. 6, p. 066 025, Apr. 2017, Publisher: IOP Publishing, ISSN: 0029-5515. DOI: 10.1088/1741-4326/aa6939. [Online]. Available: <https://dx.doi.org/10.1088/1741-4326/aa6939> (visited on 05/09/2023).
- [60] L. Hesslow, O. Embréus, O. Vallhagen, and T. Fülöp, “Influence of massive material injection on avalanche runaway generation during tokamak disruptions,” *Nuclear Fusion*, vol. 59, no. 8, p. 084 004, Jun. 2019, Publisher: IOP Publishing, ISSN: 0029-5515. DOI: 10.1088/1741-4326/ab26c2. [Online]. Available: <https://dx.doi.org/10.1088/1741-4326/ab26c2> (visited on 05/09/2023).
- [61] M. Lehnen, D.J. Campbell, D. Hu, *et al.*, *R&d FOR RELIABLE DISRUPTION MITIGATION IN ITER*, 2018. [Online]. Available: [chrome - extension : //efaidnbmninnibpcapjpcglclefindmkaj/https://nucleus.iaea.org/sites/fusionportal/Shared%20Documents/FEC%202018/fec2018-preprints/preprint0318.pdf](chrome-extension://efaidnbmninnibpcapjpcglclefindmkaj/https://nucleus.iaea.org/sites/fusionportal/Shared%20Documents/FEC%202018/fec2018-preprints/preprint0318.pdf).
- [62] C. Reux, V. Plyusnin, B. Alper, *et al.*, “Runaway electron beam generation and mitigation during disruptions at JET-ILW,” *Nuclear Fusion*, vol. 55, no. 9, p. 093 013, Aug. 2015, Publisher: IOP Publishing, ISSN: 0029-5515. DOI: 10.1088/0029-5515/55/9/093013. [Online]. Available: <https://dx.doi.org/10.1088/0029-5515/55/9/093013> (visited on 05/08/2023).
- [63] T. C. Hender, J. C. Wesley, J. Bialek, *et al.*, “Chapter 3: MHD stability, operational limits and disruptions,” *Nuclear Fusion*, vol. 47, no. 6, S128, Jun. 2007, ISSN: 0029-5515. DOI: 10.1088/0029-5515/47/6/S03. [Online]. Available: <https://dx.doi.org/10.1088/0029-5515/47/6/S03> (visited on 05/08/2023).
- [64] E. M. Hollmann, P. B. Aleynikov, T. Fülöp, *et al.*, “Status of research toward the ITER disruption mitigation system,” *Physics of Plasmas*, vol. 22, no. 2, p. 021 802, Nov. 17, 2014, ISSN: 1070-664X. DOI: 10.1063/1.4901251. [Online]. Available: <https://doi.org/10.1063/1.4901251> (visited on 05/08/2023).
- [65] A. H. Boozer, “Theory of runaway electrons in ITER: Equations, important parameters, and implications for mitigation,” *Physics of Plasmas*, vol. 22, no. 3, p. 032 504, Mar. 10, 2015, ISSN: 1070-664X. DOI: 10.1063/1.4913582. [Online]. Available: <https://doi.org/10.1063/1.4913582> (visited on 05/08/2023).
- [66] G. Papp, T. Fülöp, T. Fehér, *et al.*, “The effect of ITER-like wall on runaway electron generation in JET,” *Nuclear Fusion*, vol. 53, no. 12, p. 123 017, Nov. 2013, Publisher: IOP Publishing and International Atomic Energy Agency, ISSN: 0029-5515. DOI: 10.1088/0029-5515/53/12/123017. [Online]. Available: <https://dx.doi.org/10.1088/0029-5515/53/12/123017> (visited on 05/08/2023).
- [67] G. Papp, M. Drevlak, T. Fülöp, and P. Helander, “Runaway electron drift orbits in magnetostatic perturbed fields,” *Nuclear Fusion*, vol. 51, no. 4, p. 043 004, Mar. 2011, ISSN: 0029-5515. DOI: 10.1088/0029-5515/51/4/043004. [Online].

- Available: <https://dx.doi.org/10.1088/0029-5515/51/4/043004> (visited on 05/08/2023).
- [68] M. Gobbin, L. Li, Y. Q. Liu, *et al.*, “Runaway electron mitigation by 3d fields in the ASDEX-upgrade experiment,” *Plasma Physics and Controlled Fusion*, vol. 60, no. 1, p. 014036, Nov. 2017, Publisher: IOP Publishing, ISSN: 0741-3335. DOI: 10.1088/1361-6587/aa90c4. [Online]. Available: <https://dx.doi.org/10.1088/1361-6587/aa90c4> (visited on 05/08/2023).
- [69] C. Sommariva, E. Nardon, P. Beyer, M. Hoelzl, G. T. A. Huijsmans, and J. E. T. Contributors, “Electron acceleration in a JET disruption simulation,” *Nuclear Fusion*, vol. 58, no. 10, p. 106022, Aug. 2018, Publisher: IOP Publishing, ISSN: 0029-5515. DOI: 10.1088/1741-4326/aad47d. [Online]. Available: <https://dx.doi.org/10.1088/1741-4326/aad47d> (visited on 05/08/2023).
- [70] L. Zeng, H. R. Koslowski, Y. Liang, *et al.*, “Experimental observation of a magnetic-turbulence threshold for runaway-electron generation in the TEXTOR tokamak,” *Physical Review Letters*, vol. 110, no. 23, p. 235003, Jun. 5, 2013, Publisher: American Physical Society. DOI: 10.1103/PhysRevLett.110.235003. [Online]. Available: <https://link.aps.org/doi/10.1103/PhysRevLett.110.235003> (visited on 05/08/2023).
- [71] P. Aleynikov and B. N. Breizman, “Theory of two threshold fields for relativistic runaway electrons,” *Physical Review Letters*, vol. 114, no. 15, p. 155001, Apr. 14, 2015, Publisher: American Physical Society. DOI: 10.1103/PhysRevLett.114.155001. [Online]. Available: <https://link.aps.org/doi/10.1103/PhysRevLett.114.155001> (visited on 02/09/2023).
- [72] C. Paz-Soldan, N. W. Eidietis, Y. Q. Liu, *et al.*, “Kink instabilities of the post-disruption runaway electron beam at low safety factor,” *Plasma Physics and Controlled Fusion*, vol. 61, no. 5, p. 054001, Mar. 2019, Publisher: IOP Publishing, ISSN: 0741-3335. DOI: 10.1088/1361-6587/aafd15. [Online]. Available: <https://dx.doi.org/10.1088/1361-6587/aafd15> (visited on 04/28/2023).
- [73] C. Paz-Soldan, C. Reux, K. Aleynikova, *et al.*, “A novel path to runaway electron mitigation via deuterium injection and current-driven MHD instability,” *Nuclear Fusion*, vol. 61, no. 11, p. 116058, Oct. 2021, Publisher: IOP Publishing, ISSN: 0029-5515. DOI: 10.1088/1741-4326/ac2a69. [Online]. Available: <https://dx.doi.org/10.1088/1741-4326/ac2a69> (visited on 04/28/2023).
- [74] Y. Q. Liu, P. B. Parks, C. Paz-Soldan, C. Kim, and L. L. Lao, “MARS-f modeling of post-disruption runaway beam loss by magnetohydrodynamic instabilities in DIII-d,” *Nuclear Fusion*, vol. 59, no. 12, p. 126021, Oct. 2019, Publisher: IOP Publishing, ISSN: 0029-5515. DOI: 10.1088/1741-4326/ab3f87. [Online]. Available: <https://dx.doi.org/10.1088/1741-4326/ab3f87> (visited on 04/28/2023).

- [75] C. Reux, C. Paz-Soldan, P. Aleynikov, *et al.*, “Demonstration of safe termination of megaampere relativistic electron beams in tokamaks,” *Physical Review Letters*, vol. 126, no. 17, p. 175 001, Apr. 30, 2021, Publisher: American Physical Society. DOI: 10.1103/PhysRevLett.126.175001. [Online]. Available: <https://link.aps.org/doi/10.1103/PhysRevLett.126.175001> (visited on 04/28/2023).
- [76] Z. Y. Chen, Z. F. Lin, D. W. Huang, *et al.*, “Suppression of runaway electrons by mode locking during disruptions on j-TEXT,” *Nuclear Fusion*, vol. 58, no. 8, p. 082 002, Jun. 2018, Publisher: IOP Publishing, ISSN: 0029-5515. DOI: 10.1088/1741-4326/aab2fc. [Online]. Available: <https://dx.doi.org/10.1088/1741-4326/aab2fc> (visited on 05/08/2023).
- [77] Z. H. Jiang, X. H. Wang, Z. Y. Chen, *et al.*, “Simulation of runaway electrons, transport affected by j-TEXT resonant magnetic perturbation,” *Nuclear Fusion*, vol. 56, no. 9, p. 092 012, Jul. 2016, Publisher: IOP Publishing, ISSN: 0029-5515. DOI: 10.1088/0029-5515/56/9/092012. [Online]. Available: <https://dx.doi.org/10.1088/0029-5515/56/9/092012> (visited on 05/08/2023).
- [78] J. Mlynar, O. Ficker, E. Macusova, *et al.*, “Runaway electron experiments at COMPASS in support of the EUROfusion ITER physics research,” *Plasma Physics and Controlled Fusion*, vol. 61, no. 1, p. 014 010, Nov. 2018, Publisher: IOP Publishing, ISSN: 0741-3335. DOI: 10.1088/1361-6587/aae04a. [Online]. Available: <https://dx.doi.org/10.1088/1361-6587/aae04a> (visited on 05/08/2023).
- [79] L. Xue, G. Y. Zheng, X. R. Duan, *et al.*, “Hot VDE investigation of the negative triangularity plasmas based on HL-2m tokamak,” *Fusion Engineering and Design*, vol. 143, pp. 48–58, Jun. 1, 2019, ISSN: 0920-3796. DOI: 10.1016/j.fusengdes.2019.03.103. [Online]. Available: <https://www.sciencedirect.com/science/article/pii/S0920379619304363> (visited on 05/09/2023).
- [80] Y. Nakamura, R. Yoshino, N. Pomphrey, and S. Jardin, “P-collapse-induced vertical displacement event in high p tokamak disruption,” *Plasma Physics and Controlled Fusion*, vol. 38, no. 10, pp. 1791–1804, 1996, ISSN: 0741-3335. DOI: 10.1088/0741-3335/38/10/007.
- [81] Y. Nakamura, R. Yoshino, Y. Neyatani, *et al.*, “Mechanism of vertical displacement events in JT-60u disruptive discharges,” *Nuclear Fusion*, vol. 36, no. 5, pp. 643–656, 1996, ISSN: 0029-5515. DOI: 10.1088/0029-5515/36/5/I10.
- [82] V. E. Lukash, A. B. Mineev, and D. K. Morozov, “Influence of plasma opacity on current decay after disruptions in tokamaks,” *Nuclear Fusion*, vol. 47, no. 11, p. 1476, Oct. 2007, ISSN: 0029-5515. DOI: 10.1088/0029-5515/47/11/009. [Online]. Available: <https://dx.doi.org/10.1088/0029-5515/47/11/009> (visited on 05/09/2023).

- [83] O. Gruber, K. Lackner, G. Pautasso, U. Seidel, and B. Streibl, “Vertical displacement events and halo currents,” *Plasma Physics and Controlled Fusion*, vol. 35, B191–B204, SB 1993, ISSN: 0741-3335. DOI: 10.1088/0741-3335/35/SB/015.
- [84] R. Fitzpatrick, “A simple ideal magnetohydrodynamical model of vertical disruption events in tokamaks,” *Physics of Plasmas*, vol. 16, no. 1, p. 012506, Jan. 27, 2009, ISSN: 1070-664X. DOI: 10.1063/1.3068467. [Online]. Available: <https://doi.org/10.1063/1.3068467> (visited on 05/09/2023).
- [85] F. J. Artola, C. R. Sovinec, S. C. Jardin, M. Hoelzl, I. Krebs, and C. Clauser, “3d simulations of vertical displacement events in tokamaks: A benchmark of m3d-c1, NIMROD, and JOREK,” *Physics of Plasmas*, vol. 28, no. 5, p. 052511, May 24, 2021, ISSN: 1070-664X. DOI: 10.1063/5.0037115. [Online]. Available: <https://doi.org/10.1063/5.0037115> (visited on 05/09/2023).
- [86] N. W. Eidietis and D. A. Humphreys, “A diffusive model for halo width growth during vertical displacement events,” *Nuclear Fusion*, vol. 51, no. 7, p. 073034, Jun. 2011, ISSN: 0029-5515. DOI: 10.1088/0029-5515/51/7/073034. [Online]. Available: <https://dx.doi.org/10.1088/0029-5515/51/7/073034> (visited on 05/20/2023).
- [87] D. A. Humphreys and A. G. Kellman, “Analytic modeling of axisymmetric disruption halo currents,” *Physics of Plasmas*, vol. 6, no. 7, pp. 2742–2756, Jul. 1, 1999, ISSN: 1070-664X. DOI: 10.1063/1.873231. [Online]. Available: <https://doi.org/10.1063/1.873231> (visited on 05/20/2023).